Slip in Entangled Polymer Solutions

Vijay Mhetar and L. A. Archer*

Department of Chemical Engineering, Texas A&M University, College Station, Texas 77843

Received September 8, 1997; Revised Manuscript Received July 1, 1998

ABSTRACT: Slip in entangled polymer solutions was studied using a plane−Couette shear flow cell. On a bare silica surface, a log−log plot of slip velocity vs shear stress displayed several power law regimes. Slip behavior was observed to be a strong function of the chemical nature of the surface. On a low-energy surface obtained by grafting octadecyltrichlorosilane onto a silica surface, the slip velocity was found to be essentially proportional to the shear stress to the first power up to a moderate stress. At higher stresses, slip velocity was found to be a strong function of shear stress on both bare and grafted silica surfaces. At high stresses, the evidence of enhanced concentration fluctuations was detected. Concentration fluctuations were observed to be strongly influenced by the interaction between the polymer and the surface. A scaling model is developed to estimate the frictional drag on a probe polymer chain (*N*-mer) pulled by one of its ends through an entangled polymer (*P*-mers). This model takes into account changes in the probe chain conformation and relaxation processes of the probe and the surrounding chains. The model is extended to study slip of an entangled polymer over a weakly grafted solid surface, and its predictions are found to be in good agreement with the experimental results.

1. Introduction

The local velocity of entangled polymer fluids near solid boundaries has been the subject of much speculation in recent years.[1] The consensus now seems to be that, unlike simple small-molecule liquids, polymers violate the no-slip condition when wall shear stresses exceed a value around 0.1 MPa in entangled melts sheared over metal surfaces. Migler et al.[2] for example recently reported measurements of nonzero fluid velocities at a stationary solid surface using evanescent wave induced fluorescence combined with fringe pattern fluorescence recovery after photobleaching. Archer et al.[3] reported "direct" measurements of slip in entangled polystyrene solutions within a few micrometers of a solid surface using micrometer-sized tracer particles. Indirect evidence of slip has also emerged from macroscopic characterization of flow curves in capillary flow rheometers.[4,5] Time-dependent oscillations in pressure drop observed when polymer fluids flow through narrow channels at fixed flow rates are also believed to be caused by a stick−slip type hydrodynamic boundary condition.[4,6] Data from several of these studies show that the critical shear stress for apparent slip in entangled melts is virtually independent of molecular weight for a given polymer type.[4,6] In entangled solutions, the critical stress for apparent slip is somewhat lower and depends strongly on concentration.[8]

That slip occurs in entangled polymer fluids is not surprising, however. It has long been known for instance that the configurational entropy of a macromolecule close to a solid surface is lower than that in a bulk polymeric fluid.[9,10] In the absence of specific intermolecular interactions between the macromolecule and surface, the entropy penalty for residence near the surface is prohibitive and the equilibrium density of surface chains is consequently low. Depending on the material in contact with the surface, there are at least three possible consequences of a depletion layer at the polymer−solid interface. First, if the material is a polydisperse melt, the available space at the surface is occupied by lower molecular weight molecules. Second, if the polymer is dissolved in a marginal solvent, the available space will be occupied mostly by solvent molecules. Third, for near-monodisperse melts the surface consists of microscopic patches of polymer on an otherwise bare substrate. Apparent slip is favored in the first two situations because there is a mismatch in rheological properties of the surface layer and the bulk polymer. In the third situation an apparent violation of the no-slip condition could occur under shear if flow causes the void spaces to grow at the expense of polymer patches. This last type of slip is fundamentally different from the first two types because "true" slip governed by the "bare" friction between polymer segments and the surface occurs. For an ideal surface the bare friction coefficient is η_s/a; slip by the last mechanism would therefore result in huge slip lengths $b_{ideal} = (\eta_p/\eta_s)a$, independent of shear stress. Slip behavior of entangled polymers over low energy, nearly nonadsorbing surfaces appears to follow this mechanism qualitatively.[11] Evidence for apparent slip due to surface void formation has also been reported by Chen et al.[12] in entangled polystyrene melts and by Archer et al.[13] in unentangled polystyrene and supercooled α-D-glucose.

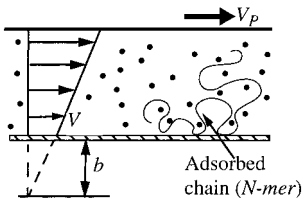

Figure 1. Polymer melt sheared over an ideal weakly grafted surface. There exists finite slip velocity, V, at the polymer−wall interface. As extrapolation length, $b \equiv V/\dot{\gamma}$, is much larger than the size of the grafted chain, it feels uniform velocity V.

The tendency for polymers to slip against solid substrates exists even when polymer−surface interactions are sufficiently strong to favor adsorption. In this case slip is favored because the relaxation dynamics of surface and bulk molecules are dissimilar. Consider a long macromolecule (*N*-mer) attached to a surface in

S0024-9297(97)01339-9 CCC: $15.00
Published on Web 09/01/1998

contact with an entangled polymer (P-mer) melt or solution. Because it is tethered to a macroscopic surface, the N-mer cannot relieve stress by simple reptational diffusion. Rather, it must relax either by arm retraction (AR), wherein the N-mer withdraws itself down the tube formed by its neighbors and escapes into a new tube,[14] or by constraint release (CR), where the N-mer relaxes in a series of impulsive Rouse-like jerks caused by reptational relaxation of neighboring bulk chains.[15] If the P-mer relaxes by AR, its relaxation time is $\tau_{AR} \approx \tau_1 N^2 \exp(15N/8N_e)$; its relaxation time by CR is[15] $\tau_{CR} \approx \tau_1 N^{2.4\pm0.1} P^{2\pm0.2} N_e^{-2\pm0.3}$, where τ_1 is the monomeric relaxation time and N_e is the average number of monomers between entanglements. In the usual situation ($N \approx P$; $N \gg N_e$) relaxation by either mechanism yields a relaxation time considerably larger than the reptation time for bulk chains $\tau_{Rep} \approx \tau_1 P^{3.4\pm0.1} N_e^{-1}$.[16] Surface polymer molecules are therefore much more easily oriented by flow than bulk ones, which favors flow-induced disentanglement at moderate flow rates and creates the appearance of slip at the walls.

The critical shear force F^* required to disentangle a single surface macromolecule N monomers long (N-mer) from an entangled melt of long molecules P monomers long (P-mer) has been estimated by Brochard-Wyart and deGennes[17,18] and by Ajdari et al.[19] to be $F^* = kT/D_e$, where $D_e = N_e^{1/2}a$ is the average distance between entanglements. If the density of polymer molecules at a surface ν is lower than or equal to $\nu_o \equiv 1/Na^2$, surface molecules can be treated as noninteracting, and the critical shear stress required for apparent slip by flow-induced disentanglement is $\sigma^* = \nu F^* = kT/NN_e^{1/2}a^3 \sim G_e N_e^{1/2}/N$, in the limit $\nu_o = 1/Na^2$ and $N = P$. Here G_e is the plateau modulus of the polymer.

The objective of the present study is 2-fold: first, to determine experimentally how apparent slip in entangled polymer solutions in good solvents depends on shear stress and entanglement density; and, second, to propose a scaling model to describe slip of an entangled polymer over a weakly grafted solid surface. Polymer solutions are chosen in this work for several reasons. First, experiments can be done at ambient temperature; second, high molecular weight narrow-size distribution polymers can be conveniently studied; and, third, the entanglement density of polymers under study can be varied by adjusting the solution concentration. In addition, for the specific polymer/solvent pair chosen (polystyrene/diethyl phthalate) the longest molecular relaxation times are conveniently long that slip in virtually all wall shear stress regimes can be investigated using a simple plane−Couette shear cell.

2. Experiments

2.1. Materials. All solutions studied consist of narrow molecular weight distribution (MWD) polystyrenes (PS) dissolved in diethyl phthalate (DEP), a good solvent of low volatility. The polymers were purchased from Polymer Source, Inc., and have molecular weights $\bar{M}_w = 2.12 \times 10^6$ and $\bar{M}_w = 6.85 \times 10^6$ with a polydispersity index $\bar{M}_w/\bar{M}_n = 1.04$. Solutions were prepared by dissolving desired amounts of both PS and DEP in excess toluene. The toluene acts as a cosolvent and reduces the viscosity of the solution, facilitating faster dissolution of the polymer. To prepare the solutions for optical microscopy, a small amount of 1.5 μm diameter spherical silica tracer particles were added to PS/DEP mixtures in toluene. The toluene was allowed to evaporate at room temperature for several weeks. The last traces of toluene were vacuum evaporated at (50 °C) for about 48 h. The compositions, c, of all solutions studied are listed in Table 1.

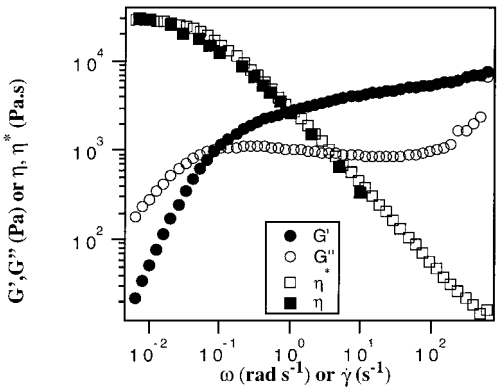

Figure 2. Frequency-dependent storage G' and loss G'' moduli for PS2.12M20% solution at 25 ± 0.5 °C. Also shown are the dynamic and steady viscosity vs frequency and shear rate, respectively. Measurements were performed with a strain amplitude of 7%.

Table 1. Molecular Characteristics and Rheological Parameters of Polystyrene Solutions

solution	$\bar{M}_w$	c (g/g)	N/N_e	η_0 (Pa·s)	G_e (Pa)	τ_{Rep} (s)
PS2.12M10%	2.12×10^6	0.1	12	220	920	0.6
PS2.12M20%	2.12×10^6	0.2	23	28120	4625	15.2
PS6.85M5%	6.85×10^6	0.05	19	90	173	1.3
PS6.85M10%	6.85×10^6	0.1	39	5400	1046	12.9

Prior to the slip measurements, the rheological properties of all test solutions were characterized by small-amplitude oscillatory shearing and steady shear measurements. Both measurements were performed using a Paar Physica Universal Dynamic Spectrometer (UDS), equipped with stainless steel cone-and-plate fixtures (25 mm diameter; 1° cone angle). Typical frequency-dependent storage and loss modulii for PS2.12M20% solution are shown in Figure 2. Also shown are the complex viscosity and steady shear viscosity versus frequency and shear rate, respectively. Rheological properties of interest for all the test solutions are listed in Table 1.

2.2. Methods. Slip measurements were performed using a plane−Couette shear cell described in detail elsewhere.[20] Briefly, the Couette cell consisted of two glass plates supported by metal frames. The lower glass plate was held stationary, whereas the upper plate was moved with the aid of a microstepper motor to impose the desired shear. The cell was designed to fit between the collimator and objective of a fixed-stage optical/fluorescent microscope capable of performing measurements with a spatial resolution of 0.5 μm. A video camera interfaced with a time lapse video recorder was used to measure the time-dependent motion of tracer particles initially resting on the stationary shear cell window. Slip velocities were deduced from this information. A gap of 500 μm was employed in all the measurements. Sample aspect ratios (gap/width) never exceeded 0.01, and all measurements were performed close to the center of the shear cell to eliminate the effect of secondary flow[20] on slip measurements.

An important concern in all tracer particle slip measurements is that slip can only be measured to within some unknown number of particle diameters from a surface. The error this causes in slip velocity measurements depends on the magnitude of the slip length at the conditions of the measurements. In section 5 the theoretical lowest slip length for an entangled polymer melt over a weakly grafted surface is shown to be $b_0 = Na$, where $a \approx 3$ Å is the monomer length. A reasonable estimate for an entangled solution in a good solvent is $b_0 = cNa$. For the polymer solutions used in this study this corresponds to a minimum slip length of around 0.5 μm, suggesting that errors could be large at very low stresses. To estimate the magnitude of error caused by the finite tracer particle size, we performed some preliminary experiments using nanosized (mean diameter, 24 nm) fluorescent polystyrene tracer particles. Because these tracer particles are polystyrene, the polymer used for the experiments

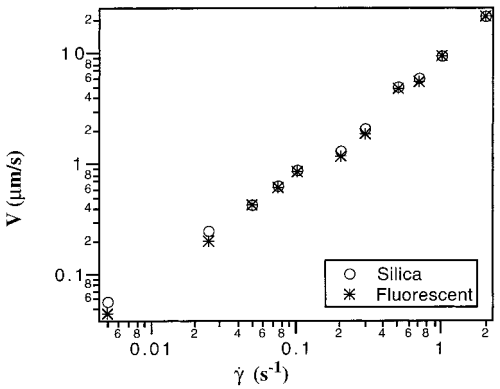

Figure 3. Comparison between slip velocities obtained using 1.5 μm diameter silica tracer particles and that obtained using 26 nm fluorescent tracer particles as a function of real shear rate.

was a 10% solution of a narrow MWD poly(ethylene oxide) ($\bar{M}_w = 1.40 \times 10^6$, $\bar{M}_n = 1.23 \times 10^6$) in water. Poly(ethylene oxide) solutions were seeded with a small quantity of 1.5 μm diameter silica particles and 24 nm fluorescent particles prior to study. The same video microscopy technique described earlier (except with a fluorescence option installed on the microscope) was used to deduce slip velocities from the time-dependent motion of both types of particles. Results are compared in Figure 3. It is apparent that the slip velocities measured using both methods are virtually identical over the entire range of shear rates studied. The mean difference in slip lengths is around 1 μm, which is close to the silica tracer particle diameter. Since one of the objectives of this study is to evaluate the detailed predictions of a scaling model, it is significant that the slip velocities determined using both particle types show the same dependence on shear rate. The fluorescence microscope used in this part of the study performs measurements in a 180° or backscattering configuration. Thus the fluorescence tracer particle technique developed here provides a new, direct method for measuring slip near metal and other opaque surfaces.

3. Results and Discussion

3.1. Slip in Entangled Polymer Solutions. Apparent slip velocities were deduced from the motion of a tracer particle close to the stationary bottom surface. Slip velocities were determined from the long-time slope of the displacement versus time plot at different nominal shear rates $\dot{\gamma}_{app}$. Plots of slip velocity, V, as a function of shear stress, σ, for all the test solutions are shown in Figure 4a−d. The shear stress, σ, was computed from the real shear rate $\dot{\gamma} = (VP - 2V)/d$ and shear viscosity results from steady shear rheometry measurements. From Figure 4a−d, it is apparent that the σ versus V relationship is highly nonlinear and can be subdivided into several near-power law regimes.

(a) At low stresses we find $V \sim \sigma^{1.0}$. The slip behavior in this regime can therefore be characterized by a single constant, slip length b_0. Experimental values of b_0 for all the solutions studied are reported in Table 2. The small magnitude of b_0 indicates large friction due to the surface adsorbed chains. The results indicate that b_0 depends on molecular weight and concentration as $b_0 \sim cM$. Slip measurements on narrow MWD polystyrene melts in the limit of low stress[21] indicate that $b_0 \sim M^{1.12}$. Thus linear dependence of b_0 on molecular weight appears to hold for polymer melts as well as for

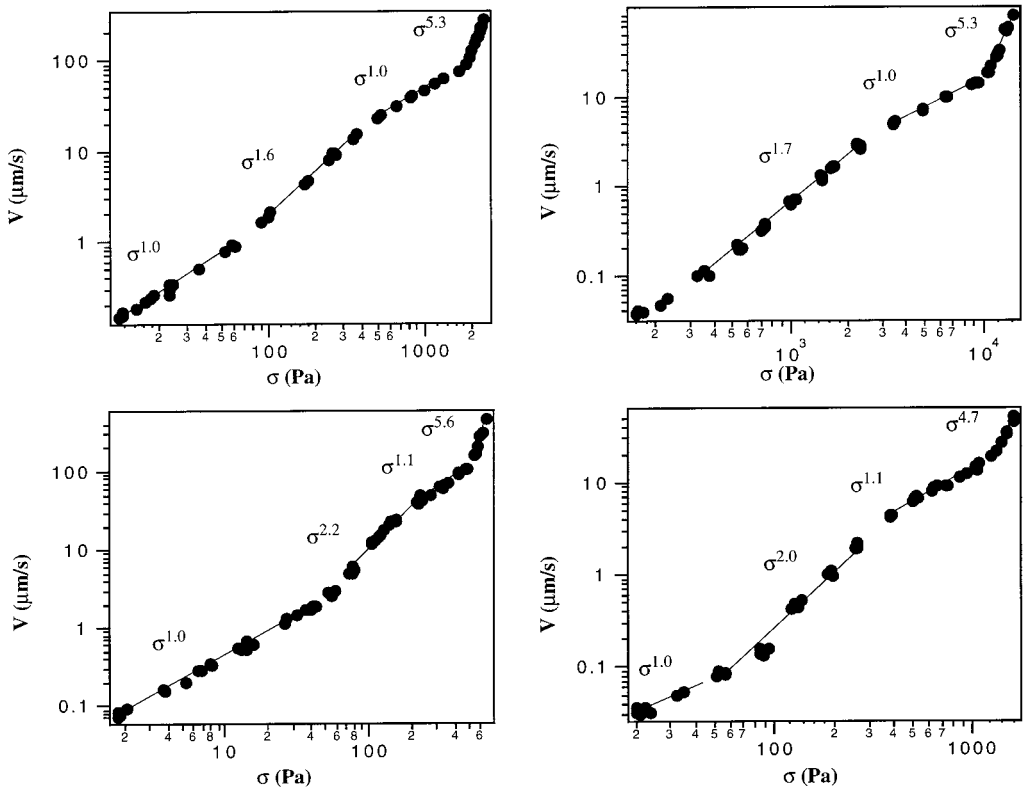

Figure 4. Typical plots of slip velocity (V) vs shear stress (σ) for (a, top left) PS2.12M10%, (b, top right) PS2.12M20%, (c, bottom left) PS6.85M5%, and (d, bottom right) PS6.85M10% solutions. The composition and linear viscoelastic properties of all the solutions are described in Table 1. The slip velocities were determined from the long-time slope of the displacement vs time plots. (i) Linear slip regime in the limit of low stress. This slip regime can be thus characterized by a constant slip length b_0. (ii) Stronger than linear dependence of V on σ in this regime likely due to the deformation of the surface adsorbed chains. (iii) Intermediate linear slip regime observed at moderate stresses. The slip behavior can be described by a constant slip length (b_m). (iv) Strong slip regime observed beyond the threshold stress σ^* characterized by a strong dependence of V on σ.

Table 2. Parameters for Describing Slip and Concentration Fluctuations in Polystyrene Solutions

solution	b_0 (μm)	b_m (μm)	σ^* (Pa)	σ^*/G_e	$\dot{\gamma}_0$ (s^{-1})	$\dot{\gamma}_{cf}$ (s^{-1})
PS2.12M10%	2.9	10.0	1870	2.0	0.20	?
PS2.12M20%	?	41.9	10460	2.3	0.01	3.5
PS6.85M5%	3.8	16.2	545	3.1	0.5	?
PS6.85M10%	8.2	68.2	1220	1.2	0.02	4.0

solutions. This linear regime could be observed only in three out of four solutions studied due to limitations on the lowest shear rate that could be imposed. The shear rate $\dot{\gamma}_0$ at which the linear regime ceases is also tabulated in Table 2. $\dot{\gamma}_0$ is seen to be lower than the inverse of the longest relaxation time of the bulk chains (τ_{Rep}) for all solutions studied. However, an approximate relation between $\dot{\gamma}_0$ and τ_{Rep} (deduced from the terminal relaxation of step strain experiment at low strain ($\gamma \approx 0.1$)) can be inferred from the experimental results: $\dot{\gamma}_0 \approx A(N_e/N)\tau_{Rep}^{-1}$. The constant A takes a value of 3.2 ± 0.3 for the PS2.12M solutions and a value of 11.2 ± 1.15 for PS6.85M solutions. The constraint release relaxation time of a N-mer immersed in a sea of other N-mers is $\tau_{CR} \approx \tau_{Rep}(N)(N/N_e)$. Since the dominant mechanism for the relaxation of polymer chains adsorbed onto a solid surface is constraint release, this result suggests that surface adsorbed chains may play an important role in the apparent slippage of entangled polymers.

(b) For shear rates $\dot{\gamma} > \dot{\gamma}_0$, slip velocities were observed to scale as $V \sim \sigma^{1.9\pm0.2}$ for all solutions studied. This stronger than linear dependence suggests a decrease in the efficiency of surface adsorbed chains to prevent slip. Since $1/\dot{\gamma}_0$ is approximately the constraint release relaxation time of the adsorbed polymer chains, $\dot{\gamma} > \dot{\gamma}_0$ causes these chains to deform under shear.

(c) Another linear regime $V \sim \sigma^{1.1\pm0.1}$ is found at higher stresses. This regime is characterized by a constant slip length b_m. The linear dependence again suggests a constant friction coefficient of the surface adsorbed chains within this regime. The magnitude of slip length in this regime can be summarized by $b_m = b_0(1/4)(N/N_e) \sim c^2N^2$ for all solutions studied.

(d) At stresses exceeding a critical value σ^*, the slip velocity is observed to increase very rapidly with shear stress $V \sim \sigma^{5.2\pm0.3}$. Values of σ^* for all the test solutions are presented in Table 2. The critical stress for each solution could be related to its bulk plateau modulus, G_e, by $\sigma^* \approx 2.15 \pm 0.55G_e$; G_e is here computed from the zero shear viscosity and reptation time as $G_e \approx 2.5\eta_0/\tau_{Rep}$.[16] Dependence of the critical stress for strong slip on the plateau modulus is consistent with results from capillary extrusion experiments on melts,[22] for which $\sigma^* \approx 0.4 - 0.5G_e$, and stress required for the onset of sharkskin in polyethylene solutions,[8] for which $\sigma^* \approx 1.73G_e$. Despite the strong increase of V with σ, the ultimate slip lengths measured are significantly lower than the theoretical bare surface slip lengths b_∞, which should be of the order of a millimeter or so for the PS solutions used here.

At shear stresses about twice σ^*($Wi \equiv \tau_{Rep}\,\dot{\gamma} \geq 50$) in regime d, we find evidence of a novel type of composition fluctuation enhancement that appears to emanate from the shearing surfaces and travel into the bulk fluid under shear. Enhanced fluctuations show up in the video micrographs as well-defined ripple patterns with ripples tilted away from the flow direction (Figure 5a–d). For $Wi \approx 50$ the ripple pattern emerged in PS2.12M20% solutions at a shear strain close to 8.0. After the cessation of flow, the pattern became progressively less defined and eventually disappeared in about 30–120 s, depending on the polymer molecular weight and concentration. The time constant for the disappearance is thus comparable to the longest relaxation time of the solution. Fast Fourier transforms (FFT) of the microscopy images are shown in the inset to the figures. At low shear rates (Figure 5a) the micrograph and its Fourier transforms are consistent with a structureless isotropic fluid. At higher shear rates (Figure 5b–d) a well-defined *butterfly* FFT pattern emerges. This pattern is characterized by a dark region along the neutral direction and enhanced scattering along the direction of shear. Qualitatively identical results were observed for several solutions of polystyrene in tricrecyl phosphate (another good solvent for the polymer). The phenomenon of shear enhancement of composition fluctuations in a binary semidilute solution of high molar mass polymer in a poor solvent has been the subject of much interest in recent years. Direct microscopy visualization of polystyrene/dioctyl phthalate semidilute solutions (PS/DOP) under shear by Moses et al.[23] revealed rippled waves tilted with respect to the flow direction. Fourier Transformation of the micrographs yielded butterfly patterns qualitatively identical to those observed in small-angle light scattering experiments.[24] The qualitative similarity between the PS/DOP results and those described in the previous section for PS/DEP is remarkable because unlike the PS/DOP work, where PS was dissolved in a poor solvent, the latter experiments all involved polystyrene in good solvents. As such, while composition fluctuations in quiescent PS/DOP are expected to be large, only weak fluctuations are anticipated in bulk PS/DEP. That flow causes significant enhancement of composition fluctuations in PS/DEP, starting at the shearing surfaces, suggests that this picture may not be accurate near these surfaces. To pursue this point further, we investigate the effect of the chemical nature of the shearing surfaces on slip and concentration fluctuation enhancement in the next section.

3.2. Effect of Surface Treatment on Slip. In this section we explore the effect of the surface on wall-slip and concentration fluctuations. Macroscopic investigations have shown that the onset condition and magnitude of wall-slip between a polymer and a solid surface depends on the chemical nature of the surface and the interactions between polymer and surface. For certain polymer/surface combinations macroscopic slip is not observed at any level of stress, whereas in others slip is detected above a well-defined critical stress value. Polystyrene melts extruded through stainless steel slit dies for instance appear to show no macroscopic evidence of slip at any stress level.[7] Shidara and Denn have attributed this observation to possible π-bonding between aromatic groups and the metal die surface, resulting in enhanced adhesion of polymer to the die. On the other hand, beyond a well-defined critical wall shear stress polybutadiene melts require a much lower pressure drop to sustain a given flow rate through poly(tetrafluoroethylene) (PTFE) capillaries, compared to stainless steel ones.[22] Other polymers such as poly(dimethylsiloxane) extruded through fluorinated dies appear to exhibit wall-slip at any stress level.[25] Hatzikiriakos and Dealy[26] studied the flow of polyethylenes in a sliding plate rheometer with plates uniformly coated with a fluoropolymer (Dynamar). Their results

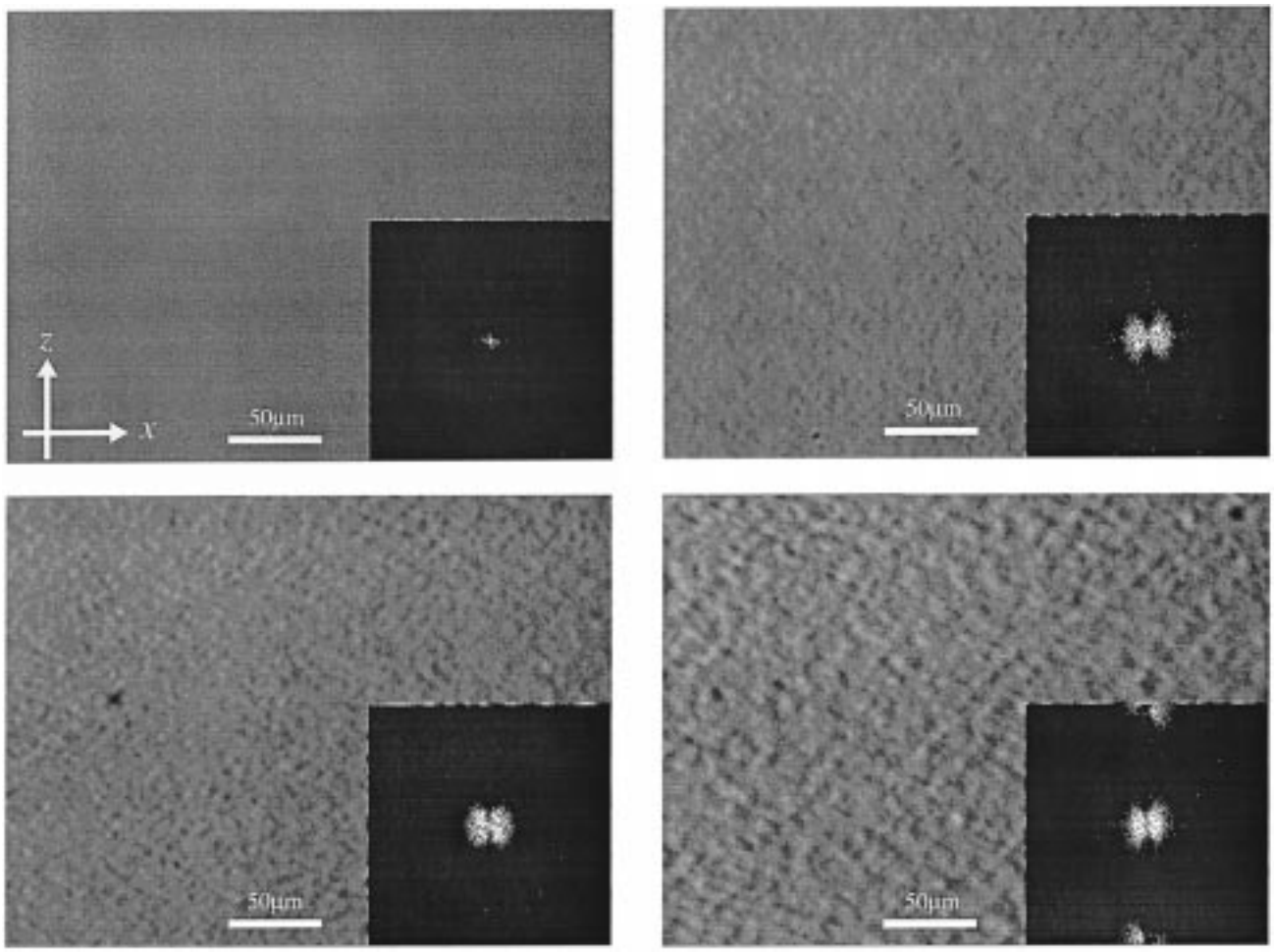

Figure 5. Microscopic images of the concentration fluctuations near the polymer−surface interface observed in the PS2.12M20% solution. Inset shows FFT of the images. Here x is the flow direction and z is the neutral direction. (a, top left) At equilibrium sample appears to be homogeneous, and FFT indicates no scattering. (b, top right) At the shear rate of 3.5 s^{-1} we clearly see the appearance of periodic structure with a length scale of about 10 μm and, at the same time, a slight scattering of FFT. (c, bottom left) At shear rate of 5 s^{-1} pronounced rippled waves begin to emerge. The waves are predominantly oriented along the neutral axis (z). FFT of the image clearly shows a butterfly pattern with dark streaks oriented along the neutral direction. (d, bottom right) At shear rate of 7 s^{-1} periodicity of the waves along the flow direction increases to about 20 μm. Strong butterfly pattern is visible in the FFT of the image.

show that apparent slip (evidenced by lower transient stresses at the wall) is triggered at lower stress levels for fluoropolymer coated plates, compared to plates made of stainless steel. To study the effect of the chemical nature of the wall surface, octadecyltrichlorosilane (OTS) was grafted onto glass. As the trichlorosilane groups of the OTS molecules react with silanol groups on silica, it produces a stable uniform layer of hydrocarbons. The recipe for grafting OTS onto silica has been described elsewhere.[27] In brief, a solvent consisting of 70 mL of hexadecane, 10 mL of carbon tetrachloride (CCl_4), and 2 mL of water saturated chlorinated solvent was prepared to which about 0.2 mL of OTS was added. Precleaned silica surfaces were soaked into this freshly prepared solution for about 2 min. Silica surfaces were then rinsed in a chloroform bath while being subjected to ultrasonic radiation to remove unreacted species. The contact angle of deionized water on OTS grafted surfaces was found to be 112 ± 3°, compared to hydrophilic glass (spontaneous spreading of water) used in the earlier part of the study.

Parts a and b of Figure 6 compare slip lengths observed on an OTS treated silica surface with those measured on bare glass at various shear stresses. At low-to-moderate shear stresses slip lengths on grafted silica were found to be a constant, independent of the shear stress. The magnitude of slip lengths were found to be larger by about a factor 2 for the PS2.12M20% and by about a factor of 3 for PS6.85M10%. At high shear rates ($\dot{\gamma} > \tau_{Rep}^{-1}$), slip lengths decreased rapidly on both surfaces and slip lengths on bare silica approach those on grafted silica. This decrease in slip length is the consequence of shear thinning, suggesting that the slip length may not be an appropriate parameter for describing slip behavior in the non-Newtonian regime. For an ideal, nonadsorbing surface the theoretical slip length is[34] $b_\infty \approx (\eta_p/\eta_{monomer})a$, which is of the order of a millimeter and is at least 2 orders of magnitude higher than the experimentally observed values on OTS grafted silica. It appears that even weak van der Waals interactions between the polymer and OTS grafted surface give rise to a friction coefficient that is much higher than the ideal monomer friction coefficient $\eta_{monomer}/a$.

To explore the effect of the surface on concentration fluctuations, an OTS grafted glass plate was substituted for one of the bare glass plates in the plane−Couette shear cell. Space resolved microscopy measurements allowed us to probe the location along the gap where the first sign of a ripple pattern could be detected. The

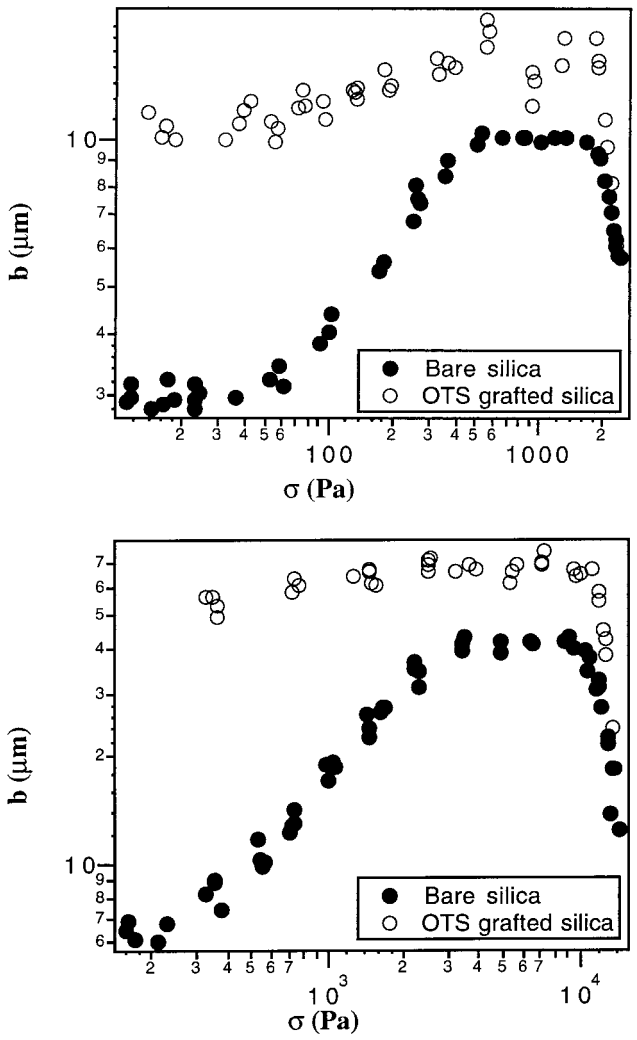

Figure 6. Comparison of slip lengths measured on bare silica with those measured on OTS grafted silica as a function of shear rate for PS2.12M20% solution.

first indication of the pattern appeared close to the bare glass with no hint of such periodic structure either in the bulk or close to the OTS grafted glass. With an increase in shear rate the pattern slowly migrated into the bulk. No sign of such rippled pattern could be detected near the OTS grafted surface until a shear rate about 4 times higher than the shear rate at which the first ripples could be seen at the ungrafted glass plate. This finding suggests that in PS/DEP composition fluctuation enhancement by shear is strongly influenced by the interaction of the polymer with the wall and is essentially an interfacial phenomena, at least initially. The gap dependence of the onset shear rate ($\dot{\gamma}_{cf}$) for the rippled pattern is summarized in Figure 7. It is apparent that $\dot{\gamma}_{cf}$ is more or less independent of the gap for gaps between 0.5 and 1 mm and weakly decreases with a decrease in gap from 0.4 to 0.1 mm, essentially in agreement with an interfacial origin of the composition fluctuation enhancement in PS/DEP. In the next section, we turn to a new scaling theory for polymer slip that fairly explains the experimental results up to regime d. The scaling theory provides a force−velocity ($F-V$) curve for a single macromolecule pulled through an entangled polymer melt that qualitatively matches recent experimental data from entangled DNA solutions. The theoretical predictions are also in agreement with most experimental data from polymer melts credited to slip. The basic physics comes from the work of Brochard-Wyart and de Gennes,[17,18] who showed that beyond a critical shear stress a transition from weak to strong slippage can occur when a melt of long macromolecules flows over an ideal surface weakly grafted with similar molecules, and from the work of Ajdari et al.[19] who introduced the paradigm of a single macromolecule pulled by one end through a sea of long macromolecules to estimate the $F-V$ diagram. The main innovation in the theory described in this paper concerns the way friction is calculated in pulled macromolecules. It is shown for example that many of the discrepancies between previous model predictions[17−19] and experimental observations are removed when the effect of entanglements are explicitly taken into account in calculating friction.

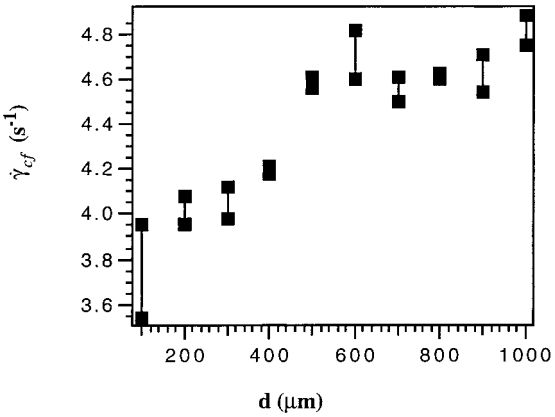

Figure 7. Effect of gap on the critical shear rate $\dot{\gamma}_{cf}$ at the inception of concentration fluctuations.

4. Scaling Model

Consider an entangled polymer melt sheared over a solid surface grafted with chemically identical polymer molecules. Such a grafted surface could arise in practical situations, such as in plastics extrusion, if a few bulk polymer molecules become attached to the extruder die wall. Although spontaneous anchoring of this sort will likely result in an ensemble of loops, trains, and tails, it should still approximate the model situation (see Figure 1) in melts when tails are substantially longer than the loop radii.[28,29] If the extrapolation length, $b \equiv V/\dot{\gamma}$, is much greater than the average size of a grafted chain, this chain experiences a uniform frictional drag force $\zeta(V)V$ due to the melt chains flowing by with velocity V. Here $\zeta(V)$ is an unknown molecular friction coefficient; V, the slip velocity; and $\dot{\gamma}$, the true shear rate.

Recently, Ajdari et al.[19] showed that the paradigm of a single probe chain pulled with constant velocity V, by one end, through an entangled polymer melt permits computation of the frictional drag force experienced by a polymer melt flowing over a weakly grafted solid surface. They computed drag force on the probe chain by estimating the stored elastic energy due to its deformation. In this paper we adopt Ajdari's pulled-chain paradigm to estimate the friction force, F, on a probe chain N monomers long, pulled with velocity, V, through a matrix of long macromolecules (P monomers per chain). We take a different approach, however, to compute the drag force on the probe chain. Instead of computing friction from elastic energy stored in the deformed probe molecule, we propose a new form for

the friction coefficient for a pulled macromolecule that depends on local structure of the pulled probe and its interactions with the surrounding molecules. Later, we compare our results with the slip experiments described in the previous section as well as with earlier theoretical predictions and with polymer slip data from several groups.

We begin by first analyzing the relaxation of a single polymer chain pulled by one end through an entangled melt. Due to the tethering at the pulling point, the mobility of such a polymer chain is severely reduced. The pulled chain is for instance unable to relax by simple reptational diffusion. Rather, its relaxation must involve arm retraction (AR), analogous to the relaxation of a star polymer, and/or constraint release (CR). In the case of arm retraction, a tethered polymer chain withdraws itself down the tube formed by its neighbors and escapes into a new tube. In CR, long polymer molecules relax in a series of impulsive Rouse-like jerks caused by reptational relaxation of neighboring chains forming the tube.[15] If relaxation occurs by AR, the relaxation time of a tail K monomers long is $\tau_{AR} \approx \tau_1 N^2 \exp(15K^2/8NN_e)$,[14] where τ_1 is the monomeric relaxation time and N_e is the average number of monomers between entanglements. If relaxation occurs by constraint release, the relaxation time of the K-mer tail can be computed using a simple physical argument: A N-mer chain in a network of P-mers will on average entangle with N/N_e neighboring P-mers, each of which is entangled with P/N_e other P-mers. Let this N-mer be pulled by one of its ends through the network of P-mers with a small velocity V (small enough that the N-mer maintains its near equilibrium conformation). Analyzing this situation Brochard et al.[15] argued that to allow the translation of the N-mer at velocity V, the surrounding entangled chains must reptate with a much faster curvilinear velocity $V(N/N_e)$. Here we suggest a different approach. When the N-mer is pulled it moves with the imposed velocity V by dragging the N/N_e P-mers chains entangled with it through their confining tubes (see Figure 9a). However since P-mers are themselves mobile, a given P-mer chain can only be dragged a short distance ($\sim V\tau_{Rep}(P)$) before it releases its entanglement with the N-mer. Because the N/N_eP-mers are entangled with P/N_e other P-mers, this dragging motion incurs a friction $f_P \equiv \zeta_P V$ per P-mer, where ζ_P is an unknown friction coefficient. ζ_P is not the usual Rouse tube friction $\zeta_P = P\zeta_m$ because the dragging motion is unidirectional and the imposed force is correlated over an entire P-mer chain (i.e. all P/N_e P-mer strands experience a directed pulling force at the same time). ζ_P is therefore not only a function of the P-mer size, but also of the number of entanglements it forms with the surrounding chains. We propose that the friction at an entanglement site formed out of a binary contact between chains of sizes A and B is $\mathrm{Min}\{A,B\}\zeta_m$. Thus for a P-mer surrounded by other P-mers, the friction per entanglement site is $\mathrm{Min}\{P,P\}\zeta_m = P\zeta_m$ and hence the friction coefficient for the entire P-mer is

$$\zeta_P = \zeta_m P(P/N_e) \tag{1}$$

Next we check eq 1 by comparing its prediction for the relaxation time of a N-mer probe in a sea of entangled P-mers with experimental results. Later we compare the zero shear viscosity computed by (1) for an ensemble of P-mers under shear flow, with the Doi−Edwards result obtained by integrating the relaxation modulus.

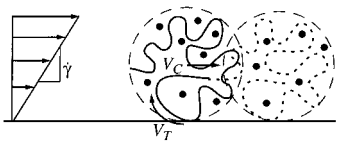

Figure 8. Polymer melt (P-mers) subjected to a simple shear flow. At low shear rates $\dot\gamma \ll 1/\tau_{Rep}(P)$ the entanglement structure is essentially unperturbed. The polymer chain moves with an average curvilinear velocity V_T, which causes its center of mass to move at velocity $V_C = V_T R/L_c(P)$. Dots represent topological constraints due to the bulk chains.

The total drag force, F, required to pull the N-mer through a sea of P-mers is by eq 1

$$F \approx \frac{N}{N_e} f_P = \frac{N}{N_e}\frac{P}{N_e} P\zeta_m V = \eta_s a V \frac{NP^2}{N_e^2} = \eta_p a V \frac{N}{P} \tag{2}$$

where, ζ_m, η_s, and η_p are the monomeric friction coefficient, monomer viscosity, and the reptation viscosity, respectively. The constraint release friction coefficient ζ_{CR} for the N-mer is therefore $\zeta_{CR} \equiv F/V \approx NP^2N_e^{-2}$, and the corresponding constraint release relaxation time τ_{CR} is $\tau_{CR} = R^2/D_{CR} \approx \tau_1 N^2P^2N_e^{-2}$; where, $D_{CR} \equiv ((kT)/\zeta_{CR})$ is the constraint release diffusion coefficient, and τ_1 is the monomeric relaxation time. This prediction for τ_{CR} is in fair agreement with experimentally observed scalings $\tau_{CR} \sim N^{2\pm0.2}P^{2.4\pm0.1}N_e^{-2\pm0.3}$.[15] Thus for a section of K monomers relaxing by constraint release we get $\tau_{CR} \approx \tau_1 K^2P^2N_e^{-2}$. Comparing τ_{CR} with τ_{AR}, we conclude that for most practical situations (typical values of $N = 10-100\ N_e$), CR is the dominant relaxation mechanism.

We now show that the zero shear viscosity computed from eq 1 is consistent with the Doi−Edwards result obtained by integrating the relaxation modulus.[30] Consider a monodisperse polymer melt (P-mers) subjected to a simple shear flow with a small shear rate $\dot\gamma \ll 1/\tau_{Rep}(P)$. The rate of energy dissipation per unit volume is $\eta_{p0}\dot\gamma^2$, where η_{p0} is the melt viscosity.[31] The dissipation due to a single P-mer, see Figure 8, can be written as $\zeta_C V_C^2 = \zeta_C R^2\dot\gamma^2$, where ζ_C is the center of mass friction coefficient and V_C is the average velocity of the center of mass. The rate of dissipation per unit volume is therefore $\zeta_C R^2\dot\gamma^2/Pa^3$ which yields $\eta_{p0} = \zeta_C/a$. When the P-mer moves by $L_c(P)$ along its curvilinear path, its center of mass moves by R. Equating dissipation rates, we get

$$\zeta_C = \zeta_P\left(\frac{V_T}{V_C}\right)^2 = \zeta_P\left(\frac{L_c(P)}{R}\right)^2 = \frac{P^3}{N_e^2}\zeta_m \tag{3}$$

where V_T is the curvilinear velocity of the P-mer. Thus the zero shear viscosity is predicted to be $\eta_{p0} = \eta_s P^3/N_e^2$, where $\eta_s = \zeta_m/a$ is the monomer viscosity.

Next we study the force−velocity diagram for the pulled N-mer in a network of P-mers. At small velocities, $V \le R(N)/\tau_{CR}(N) = V_1 = aN^{-3/2}N_e^2P^{-2}/\tau_1$, the N-mer relaxes faster than pulling perturbs it, so it maintains its equilibrium Gaussian coil configuration (*ball*) configuration (see Figure 9a) during pulling. For $V < V_1$, the force required to pull the chain is from eq 2,

$$F = F_B(N) \approx \eta_s a V N P^2 N_e^{-2} = \eta_p a V N P^{-1} \tag{4}$$

When the imposed velocity exceeds V_1, the entire probe chain is unable to relax during pulling and begins to deform. Thus for $V > V_1$, the probe chain should look

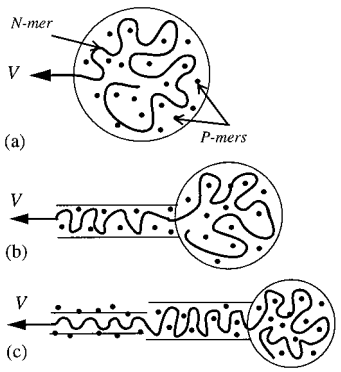

Figure 9. *N*-mer chain pulled by one of its ends, with velocity *V*, through an entangled polymer melt (*P*-mers). (a) At low velocities the probe chain moves as an unperturbed coil (ball). (b) At intermediate velocities the chain can be described as a cylinder ($N-K$ monomers) at the head and a ball (K monomers) at the tail. (c) When velocity, V, exceeds V_3, a probe chain forms a disentangled stick (J monomers) at the head followed by the cylinder and ball at the tail. Dots represent topological constraints due to the bulk chains.

like a trumpet[19] which, for the purpose of drag calculations, can be simplified into two sections; a ball at the tail (K monomers) and a cylindrical tube ($N-K$ monomers) at the head (Figure 9b). To find the friction on the cylinder, it is necessary to know its diameter. If the diameter of the cylinder, D_{Cylinder}, is larger than D_e the $(N-K)$ monomers within the cylinder must drag all the chains entangled with it to maintain the larger diameter. In such case, the friction per monomer on cylinder would be identical to the friction per monomer on ball and would be given by eq 4. On the other hand, if the diameter of the cylinder is equal to D_e, the monomers trapped within the cylinder can slide over the entangled chains instead of dragging them. In this case the friction on the cylinder ($N-K$ monomers), from eq 1, is

$$F_C(N-K) = \eta_s a V (N-K)^2/N_e \qquad (5)$$

Since the friction on the cylinder with $D_{\text{Cylinder}} = D_e$, given by eq 5, is smaller by a factor of $((N-K)N_e)/P^2$ than the friction on the cylinder with $D_{\text{Cylinder}} > D_e$ that would result from dragging the entangled chains, the diameter of the cylinder must be D_e. Obviously there will be a small crossover region between the cylinder of diameter D_e and the ball. However, since the friction coefficient for the cylinder with $D_{\text{Cylinder}} > D_e$ is identical to the friction coefficient for the ball, the friction due to the monomers within the crossover region (i.e. with $D_{\text{Cylinder}} > D_e$) can be included in the ball friction. In other words, the number of monomers, K, includes the monomers within the ball and the monomers within the crossover region, leaving ($N-K$) monomers for the cylinder. Note that we argue that the cylinder diameter results from the above principle of least friction unlike previous work based on force balance on the monomers.[15-17] The friction on the cylinder ($N-K$ monomers at the head) is given by eq 5, and the friction on the tail of K monomers comprising ball and crossover conformation is computed from eq 4, which reads

$$F_B(K) \approx \eta_s a V K P^2 N_e^{-2} = \eta_p a V K P^{-1}$$

Thus the total drag on the chain is $F = F_B(K) + F_C(N-K)$, where the subscripts B and C mean ball and entangled cylinder, respectively. The number of monomers in the ball, K, clearly depends on the imposed velocity, V; thus if $V(K) \approx R(K)/\tau_{CR}(K)$, $K \approx (a/\tau_1)^{2/3}(Ne/P)^{4/3}V^{-2/3}$. When substituted in the expression for F_B from eq 4, the $F-V$ relation for $V > V_1$ is obtained,

$$F \approx F_B \approx \eta_s a V^{1/3}(a/\tau_1)^{2/3}(N_e/P)^{-2/3} \qquad (6)$$

It is apparent that a crossover from ball-dominated to cylinder-dominated friction occurs when $K \approx N^2P^{-2}N_e$. For $N \approx P$ we get $K \approx N_e$, suggesting that the ball friction could dominate the entire regime. However, eq 4 applies under the condition that the imposed velocity $V \ll D_e/\tau_{Rep}(P) = V_2$, where $D_e = N_e^{1/2}a$ is the average distance between entanglements. As the imposed velocity approaches V_2 the P-mers entangled with the ball are dragged to a distance of about D_e, where additional entanglements are formed with the probe. For $V > V_2$ the surrounding chains therefore act as effectively permanent obstacles to the motion of the probe chain. As the surrounding chains are effectively immobile on the time scale of motion of the probe tail, its relaxation dynamics must switch from CR to AR. The number of monomers, K, within the relaxed ball should satisfy $V = R(K)/\tau_{AR}(K)$. Note that the size of the ball is very small. Thus the drag force on the entire chain for $V > V_2$ is

$$F \approx F_C(N) \approx \eta_s a V N^2/N_e \qquad (7)$$

When $V \le L_c(N)/\tau_{\text{Rouse}}(N) = a/\tau_1 N N_e^{1/2} = V_3$, the pulled chain though perturbed maintains its equilibrium contour length $L_c(N)$, where $\tau_{\text{Rouse}}(N)$ is the Rouse relaxation time of the N-mer probe. Chain stretching is avoided at these pulling velocities by a dynamic process akin to the rapid equilibration or retraction process envisioned by Doi and Edwards[30] in their description of entangled polymer relaxation dynamics following large step-strains. When the imposed velocity exceeds V_3, only J monomers, counted from the tail, can retract and remain entangled. The remaining ($N-J$) monomers next to the tethered point are stretched to form a disentangled *stick* (see Figure 9c). The friction acting on the *stick* is therefore monomeric,

$$F_S(N-J) \approx (N-J)\zeta_m V = \eta_s a V (N-J) \qquad (8)$$

For a small *stick* (i.e. $J \approx N$), however, the friction will still be dominated by the cylinder and ball friction, so $F \approx F_C(J)$. The number of monomers, J, in the cylinder and ball is a function of the imposed velocity and is given by $V(J) \approx a/\tau_1 J N_e^{1/2}$. When the stick section is small, we therefore obtain

$$F \approx F_C(J) \approx \eta_s a^3 N_e^{-2} \tau_1^{-2} V^{-1} \qquad (9)$$

This result can be interpreted as follows: for $V > V_3$ an increase in the imposed velocity causes the number of monomers in the stick ($N-J$) to increase and the number of monomers in the cylinder and ball (J) sections to decrease. Comparing eqs 8 and 9, it is evident, however, that an initial loss of monomers from the ball and cylinder sections of the probe chain to the stick actually causes a net decrease in frictional force. Thus the total drag, F, decreases as the imposed velocity V increases. This result implies that the $F-V$ diagram must have a multivalued, unstable section in this velocity regime. The unstable regime continues until

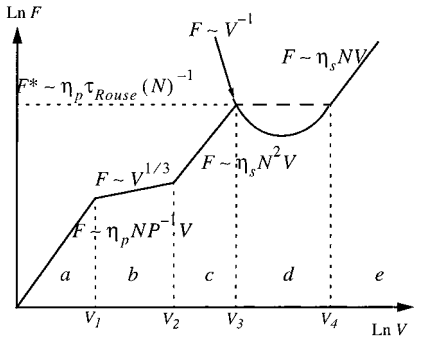

Figure 10. Force−velocity diagram for the probe chain pulled through an entangled polymer melt or solution. (a) Linear entangled friction regime ($V > V_1 = R(N)\tau_{CR}^{-1}(N)$). (b) Cylinder and ball regime when surrounding chains are mobile ($V_1 < V < V_2 = D_e/\tau_{Rep}(P)$). (c) Cylinder and ball regime when surrounding chains represent permanent obstacles ($V_2 < V < V_3 = L_c(N)/\tau_{Rouse}(N)$). (d) Stick−cylinder−ball regime ($V_3 < V < V_4 = V_3 N/N_e$). (e) Stable monomeric friction regime ($V > V_4$).

the velocity reaches $V_4 = V_3(N/N_e) = a/\tau_1 N_e^{3/2}$, such that the number of monomers in the stick is sufficiently large that the incremental increase in monomeric stick friction F_S just begins to exceed the loss friction due to shrinkage of the ball and cylinder sections:

$$F_S \approx \eta_s a N V_4 = \eta_s a N^2 N_e^{-1} V_3 \equiv F^* \qquad (10)$$

The critical force F^* required to completely disentangle the probe chain is then

$$F^* = \frac{N}{N_e^{3/2}} \frac{kT}{a} = \frac{N}{N_e} \frac{kT}{D_e} \qquad (11)$$

Significantly, the critical force in eq 11 is predicted to be larger, by a factor of N/N_e, than F^* estimates from earlier analyses.[17−20] The total drag during the unstable regime ($V_3 < V < V_4$) is

$$F = \frac{\eta_s a^3}{N_e \tau_1^2} \frac{1}{V} + \eta_s \left(N - \frac{a}{\tau_1 V N_e^{1/2}} \right) aV \qquad (12)$$

For velocities $V > V_4$, the friction is essentially due to monomeric friction of the stick

$$F \approx F_S(J) \approx F_S(N) = \eta_s a V \qquad (13)$$

5. Model Predictions and Comparison with the Experiments

The theoretical force velocity diagram is summarized in Figure 10. Recently Wirtz[32] measured the $F-V$ diagram for a single fluorescently labeled DNA probe molecule pulled by one end through a solution of entangled DNA. In these experiments the desired force was applied through a magnetic bead attached to the DNA probe (*magnetic tweezers*). The predicted $F-V$ diagram shown in Figure 10 is in qualitative agreement with the $F-V$ data reported by Wirtz.[32] This should be contrasted with previous studies[17−19] that were unable to predict $F-V$ regimes b and c in Figure 10. Also, the predicted critical force for disentanglement of the DNA probe used in Wirtz's experiment is about 11 pN, compared to the reported value of 20 pN; earlier predictions yield $F^* = 0.07$ pN.

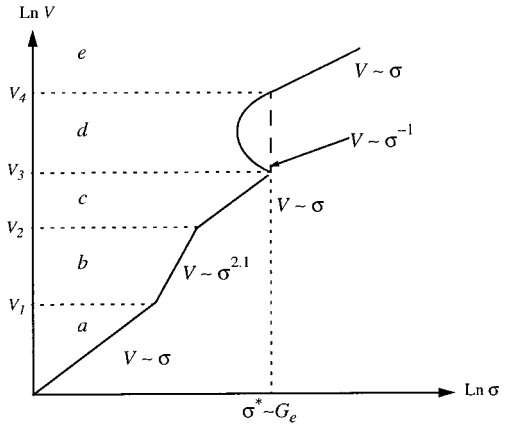

Figure 11. Slip velocity−shear stress diagram when an entangled polymer (*P*-mers) is sheared over a weakly grafted (*N*-mers) solid surface. (a) Linear slip velocity regime ($V > V_1$). (b) Cylinder and ball regime when surrounding chains are mobile ($V_1 < V < V_2$). (c) Intermediate linear slip velocity regime $V_2 < V < V_3$. (d) Unstable regime $V_3 < V < V_4$. Multiple values of slip velocities exist for the same shear stress. (e) Terminal linear slip velocity regime ($V > V_4$).

In the next section we use the force−velocity results to study slip of entangled polymers sheared over weakly grafted surfaces. For the sake of comparison with experimental results we consider the symmetric case where the length of surface and bulk chains are identical, i.e., $P = N$. We also take the graft density, the number of grafted polymer chains per unit area, to be the maximum value possible without overlap $\nu \sim (Na^2)^{-1}$. The slip length is related to the frictional drag force between surface and bulk polymer chains by, $b \equiv V/\dot{\gamma} = (\eta_p V)/\sigma = (\eta_p/\nu)(V/F)$, where $\dot{\gamma}$ and $\sigma = \nu F$ are the imposed shear rate and shear stress. Figure 11 summarizes the shear stress−slip velocity ($\sigma-V$) diagram calculated from the force−velocity results summarized in Figure 10. Here we simply enumerate the most salient features of the diagram and compare them with the results of experiments described in the previous section and also with the published experimental data. Where necessary, we also make comparisons with results from previous analyses that also attempt to describe slip in polymers.

In the limit of low σ the slip velocity is seen to be simply proportional to the wall shear stress characterized by a constant slip length $b = b_0 = Na$, compared to $b_0 \approx N_e a$ obtained by Brochard-Wyart et al.[18] Slip of narrow molecular weight distribution polystyrene melts[21] in the limit of low stress indicate $b_0 \sim N^{1.11\pm0.33}$. Results of slip measurements on polystyrene solutions summarized in Figure 4a−d indicate $b_0 \sim cN$ in agreement with the theoretical prediction. At shear rates exceeding τ_{CR}^{-1} the model predicts $V \sim \sigma^{3.0}$, which is not in agreement with the experimentally observed slip velocity scaling ($V \sim \sigma^{1.9\pm0.2}$). However, if the theoretical dependence of the constraint release time on molecular weight $\tau_{CR} \sim N^2$ is replaced by the experimental result $\tau_{CR} \sim N^{2.4}$, the theoretical slip velocity dependence on shear stress becomes $V \sim \sigma^{2.1}$, which is in good agreement with the experimental result.

Another linear regime ($V \sim \sigma$) characterized by a constant slip length, b_m, is predicted at higher stresses. The slip length is predicted to scale as $b_m \sim N^2$. Experimental results (Figure 4a−d) clearly show the presence of the second linear regime with slip lengths

($b_m \approx b_0(1/4)(N/N_e) \sim c^2N^2$), in good agreement with the theoretical prediction.

The critical shear stress required for disentanglement between bulk and surface chains is predicted to be $\sigma = \sigma^* \approx \eta_p/\tau_{Rep}(N) = G_e$, where G_e is the plateau modulus of the entangled polymer in good agreement with the experimental results (see Table 2). Experiments with linear low-density polyethylene solutions by Pomar et al.[8] indicate that $\sigma^* = 1.73\ G_e$, whereas Vinogradov et al.[22] found the experimental relation $\sigma^* \sim 0.4-0.5\ G_e$ from the capillary flow experiments on a series of polyisoprenes and polyisobutylenes. The critical shear stress is predicted to be independent of molecular weight in contrast with previous predictions[17-19] which suggest $\sigma^* \sim N^{-1}$. Extrusion studies using a series of poly(dimethylsiloxanes)[4] indicate that the critical shear stress required for the onset of macroscopic slip is indeed independent of molecular weight. In similar studies using a series of polybutadienes Lim and Schowalter[6] find $\sigma^* \cong 2$ bar compared to the predicted value of $\sigma^* \cong 2.25$ bar.

Periodic oscillations in pressure drop and/or polymer throughput rate have also been reported[6] at stresses close to σ^*, suggesting a stick−slip-like instability at stresses close to this value. This result is in accord with our prediction of multivalued slip velocities at similar stresses. Furthermore, at stress values exceeding the critical stress, experimental studies report significant reductions in the oscillation amplitude and frequency leading to nearly steady flow with a uniform macroscopic slip velocity at the walls,[4,6] again in agreement with the theoretical prediction of a stable monomeric friction regime for $F > F^*$.

6. Summary

Slip in entangled polymer solutions over a silica surface is studied. On bare silica we find a log−log plot of slip velocity vs shear stress has several power law regimes (Figure 4a−d). (i) At low shear stresses slip velocity was found to be proportional to shear stress characterized by a constant slip length which was found to scale as $b_0 \sim cN$ in agreement with the slip length data on polystyrene melts in the limit of low stresses.[21] (ii) At shear rates exceeding $\dot{\gamma}_0$, we find $V \sim \sigma^{1.9\pm0.2}$. The onset shear rate $\dot{\gamma}_0$ for this regime was found to be a function of the longest relaxation time of the solution τ_{Rep}^{-1} and the number of entanglements N/N_e. (iii) At even higher stresses we observe $V \sim \sigma^{1.1\pm0.1}$ characterized by a constant slip length b_m. The magnitude of slip length was found to be $b_m \approx b_0(1/4)(N/N_e) \sim c^2N^2$. (iv) At stresses exceeding certain critical stress σ^*, slip velocity is observed to be a strong function of shear stress given by $V \sim \sigma^{5.2\pm0.3}$. The critical stress σ^* was found to be proportional to the plateau modulus G_e of the respective solution consistent with extrusion experiments on polymer melts[22] and solutions.[8] A scaling model is proposed to estimate the frictional drag on a probe polymer chain pulled through an entangled polymer melt by one of its ends. This model takes into account changes in the chain configuration and relaxation processes of the probe and surrounding chains. The predicted force−velocity ($F-V$) diagram (Figure 10) is in qualitative agreement with recent experimental data. The model is extended to study slip of an entangled polymer over a weakly grafted ideal surface. The predictions of this model are in good to excellent agreement with the polystyrene solution experiments described in this study and also with experimental observations from several research groups.

We also report novel shear enhancement of concentration fluctuations in high molecular weight polystyrene in good solvents. Enhancement of composition fluctuations is characterized by the appearance of a periodic rippling pattern during flow microscopy measurements similar to the patterns found in semidilute solution of PS in DOP using a similar technique. The composition fluctuations reported here are unusual, however, because they appear to nucleate at the shearing surfaces and travel into the bulk. In addition, unlike the PS/DOP system where concentration fluctuation enhancement leads to strong scattering dichroism, no dichroism could be detected in our test solutions. As a result of their sensitivity to the surface details, we speculate that enhanced composition fluctuations in sheared PS/DEP might be caused by shear-induced enhanced polymer adsorption to the shearing surfaces. Such enhancement in adsorption has been reported for poly(methyl methacrylate) (PMMA) solutions in CCl_4, a poor solvent, sheared between germanium surfaces.[33]

Acknowledgment. The authors gratefully acknowledge the National Science Foundation, Faculty Early Career Program; the 3M Corp. Nontenured Faculty research grant program, and the donors of the Petroleum Research Fund, administered by the American Chemical Society, for supporting this work.

References and Notes

(1) Denn, M. M. *Annu. Rev. Fluid. Mech.* **1990**, *22*, 13.
(2) Migler, K. B.; Hervet, H.; Leger, L. *Phys. Rev. Lett.* **1993**, *70*, 287.
(3) Archer, L. A.; Larson, R. G.; Chen, Y.-L. *J. Fluid. Mech.* **1995**, *301*, 133.
(4) Kissi, N. El.; Piau, J. M. *J. Non-Newtonian Fluid Mech.* **1990**, *37*, 55.
(5) Wang, S.-Q.; Drda, P. *Macromolecules* **1996**, *29*, 4115.
(6) Lim, F. J.; Schowalter, W. R. *J. Rheol.* **1989**, *33*, 1359.
(7) Shidara, H.; Denn, M. M. *J. Non-Newtonian Fluid Mech.* **1993**, *48*, 101.
(8) Pomar, G.; Muller, S. J.; Denn, M. M. *J. Non-Newtonian Fluid Mech.* **1994**, *54*, 143.
(9) Asakura, S.; Oosawa, F. *J. Chem Phys.* **1952**, *22*, 1255.
(10) Dimarzio, E. A.; McCrackin, F. L. *J. Chem. Phys.* **1965**, *43*, 539.
(11) Inn, Y.-W.; Wang, S.-Q. *Phys. Rev. Lett.* **1996**, *76*, 467.
(12) Chen, Y.-L.; Larson, R. G.; Patel, S. S. *Rheol. Acta* **1994**, *33*, 243.
(13) Archer, L. A.; Ternet, D.; Larson, R. G. *Rheol. Acta* **1997**, *36*, 579.
(14) Doi, M.; Kuzuu, N. Y. *J. Polym. Sci., Polym. Lett. Ed.* **1980**, *18*, 775.
(15) Brochard-Wyart, F.; Ajdari, A.; Leibler, L.; Rubinstein, M.; Viovy, J. L. *Macromolecules* **1994**, *27*, 803. Ajdari. A.; Brochard-Wyart, F.; Gay, C.; deGennes, P. G.; Viovy, J. L. *J. Phys. (Paris)* **1995**, *5*, 491.
(16) Graessley, W. W. *Adv. Polym. Sci.* **1974**, *16*, 78.
(17) Brochard-Wyart, F.; deGennes, P. G. *Langmuir* **1992**, *8*, 3033.
(18) Brochard-Wyart, F.; Gay, C.; deGennes, P. G. *Macromolecules* **1996**, *29*, 377.
(19) Ajdari, A.; Brochard-Wyart, F.; deGennes, P. G.; Leibler, L.; Viovy, J. L.; Rubinstein, M. *Physica A* **1994**, *104*, 17.
(20) Mhetar, V. R.; Archer, L. A. *J. Rheol.* **1996**, *40*, 549.
(21) Henson, D. J.; Mackey, M. E. *J. Rheol.* **1995**, *39*, 359.
(22) Vinogradov, G. V.; Protasov, V. P.; Dreval V. E. *Rheol. Acta* **1984**, *23*, 46.
(23) Moses, E.; Kume, T.; Hashimoto, T. *Phys. Rev. Lett.* **1994**, *72*, 2037.
(24) Wu, X.-L.; Pine, D. J.; Dixon, P. K. *Phys Rev. Lett.* **1991**, *66*, 2408.
(25) Kissi, N. El.; Leger, L.; Piau, J.-M.; Mezghani, A. *J. Non-Newtonian Fluid Mech.* **1994**, *52*, 249.

(26) Hatzikiriakos, S. G.; Dealy, J. M. *J. Rheol.* **1991**, *35*, 497.
(27) Silberzan, P.; Leger, L.; Ausserre, D.; Benattar, J. J. *Langmuir* **1991**, *7*, 1647.
(28) Guiselin, O. *Europhys. Lett.* **1992**, *17*, 225.
(29) Semenov, A. N.; Bonet-Avalos, J.; Johner, A.; Joanny, J. F. *Macromolecules* **1996**, *29*, 2179.
(30) Doi, M.; Edwards, S. F. *The Theory of Polymer Dynamics*; Oxford University Press: Oxford, U.K., 1986.
(31) Ferry, J. D. *Viscoelastic Properties of Polymers*, 2nd ed.; Wiley: New York, 1970.
(32) Wirtz, D. *Phys. Rev. Lett.* **1995**, *75*, 2436.
(33) McGlinn, T. C.; Kuzmenka, D. J.; Granick, S. *Phys. Rev. Lett.* **1988**, *60*, 805.
(34) deGennes, P. G. *C. R. Acad. Sci.* **1979**, *288*, 219.

MA971339H